Predicting Therapeutic Response to Osimertinib Using Explainable Machine Learning: A Clinical Decision Support Framework for Precision Management of EGFR-Mutated Non-Small Cell Lung Cancer

Dr. Ohmini Krishnamurthy Rajendran

Consultant Radiologist,
KIMS Hospital and Research Centre
Bengaluru, India
Jsmnk4@gmail.com
Orcid id- 0009-0006-1516-5002

Received: 12th April, 2026; **Revised:** 5th may , 2026; **Accepted:** 10th June, 2026; **Available Online:** 14th July, 2026

Abstract

Background. Osimertinib is the standard first-line therapy for epidermal growth factor receptor (EGFR)-mutated non-small cell lung cancer (NSCLC), yet response is heterogeneous and no validated tool predicts which patients will benefit. Black-box models that forecast response are difficult to deploy because clinicians cannot interrogate their reasoning. We developed an explainable artificial intelligence (XAI) clinical decision support framework that predicts osimertinib response while exposing the features driving each prediction.

Methods. A retrospective multicenter cohort of 350 patients with EGFR-mutated NSCLC (Stage III–IV) treated with osimertinib was assembled, spanning exon 19 deletion, L858R, T790M, and uncommon mutations. The framework integrates clinical variables, CT radiomics, molecular biomarkers, and laboratory data, and was benchmarked against random forest, XGBoost, LightGBM, and an explainable boosting machine (EBM). SHapley Additive exPlanations (SHAP) and Local Interpretable Model-agnostic Explanations (LIME) provided interpretability. Performance used five-fold cross-validation and an external test set.

Results. The proposed model achieved an accuracy of 0.918, F1-score of 0.907, and area under the receiver operating characteristic (ROC) curve (AUC) of 0.954, exceeding EBM (AUC 0.921) and LightGBM (AUC 0.912). The objective response rate was 59.7% (209 of 350). Predicted responders had markedly longer progression-free survival (PFS) than predicted non-responders (median 22.5 versus 7.8 months). EGFR mutation type, tumor volume, and a composite radiomics score were the dominant predictors.

Conclusions. An explainable machine-learning framework integrating clinical, radiomic, and molecular data predicted osimertinib response accurately while preserving interpretability, supporting patient selection, early identification of non-responders, and biomarker-driven decision-making. Prospective external validation is required before clinical use.

Keywords: Osimertinib; EGFR-mutated NSCLC; Explainable Artificial Intelligence; Machine learning; Radiomics; SHAP; Progression-Free Survival; Treatment Response Prediction; Precision Oncology.

How to cite this article: Rajendran OK. Predicting Therapeutic Response to Osimertinib Using Explainable Machine Learning: A Clinical Decision Support Framework for Precision Management of EGFR-Mutated Non-Small Cell Lung Cancer. Int J Drug Deliv Technol. 2026;16(69s):1181-1189. DOI: 10.25258/ijddt.16.69s.119

1. Introduction

Lung cancer remains the leading cause of cancer death worldwide, and EGFR-mutated NSCLC represents a major molecular subset in which targeted therapy has transformed outcomes. Osimertinib, a third-generation irreversible EGFR tyrosine kinase inhibitor (TKI) active against sensitizing and T790M resistance mutations, is now standard first-line therapy after the FLAURA trial demonstrated superior progression-free and overall survival relative to earlier-generation TKIs. Despite this advance, response is not uniform: some patients progress within months, while others maintain durable disease control. Identifying these divergent trajectories before treatment begins would allow therapy to be matched to the patients most likely to benefit and would spare others avoidable toxicity and delay.

This heterogeneity arises from biology that a single variable cannot capture. EGFR mutation subtype influences benefit, with exon 19 deletions generally more responsive than L858R, and co-occurring alterations such as TP53 mutation and MET amplification shape both primary and acquired

resistance. Imaging phenotype, tumor burden, and host inflammatory markers add further prognostic information. Integrating these dimensions to predict response at the point of treatment selection is a genuine unmet need, because patients unlikely to benefit might be spared months of ineffective therapy and directed toward combination or alternative strategies.

Machine learning can integrate such high-dimensional, multimodal data, but clinical adoption has been limited by the opacity of high-performing models. Oncologists are reasonably reluctant to act on a prediction they cannot interrogate, particularly when it influences whether a patient receives standard-of-care therapy. XAI addresses this barrier by attributing each prediction to specific, clinically meaningful features, allowing the reasoning to be inspected and challenged. The distinction matters in practice: a model that reports only a probability offers little that a clinician can verify, whereas one that shows the probability rests on an exon 19 deletion, a modest tumor burden, and absent resistance co-mutations presents a rationale that maps onto established biology and can be accepted or overridden on clinical grounds.

We present an XAI clinical decision support framework that predicts osimertinib response in EGFR-mutated NSCLC by integrating clinical characteristics, CT radiomics, molecular biomarkers, and laboratory data. We benchmark it against established gradient-boosting and tree-based models, evaluate progression-free survival stratified by predicted response, and use SHAP and LIME to expose the drivers of prediction. Our aim is to show that explainability and accuracy can be achieved together in a tool suited to real clinical decision-making.

2. Literature Review

Three research streams inform this work. Clinical trials established osimertinib efficacy and characterized resistance, radiomics studies showed that CT-derived features encode molecular and prognostic information in NSCLC, and machine-learning studies demonstrated prediction of EGFR status and treatment outcome. Explainability has more recently been recognized as essential for clinical translation, yet few studies combine multimodal integration with interpretability for osimertinib response specifically. The practical consequence is a gap between models that perform well in retrospective benchmarks and tools that clinicians are willing to use, a gap that interpretability is increasingly understood to bridge.

Across this literature, recurring gaps include single-modality inputs, reliance on black-box models without explanation, and a focus on mutation detection rather than response prediction. Table 1 summarizes representative studies from 2017–2025 spanning these streams.

Table 1. Representative studies on osimertinib, radiomics, and machine learning in EGFR-mutated NSCLC.

Author	Year	Study focus	Dataset	AI/ML method	Key findings	Research gap
Soria et al.	2018	First-line osimertinib	FLAURA, 556	Statistical	Superior PFS vs older TKIs	No response prediction
Ramalingam et al.	2020	Osimertinib overall survival	FLAURA	Statistical	OS benefit confirmed	No predictive model
Leonetti et al.	2019	Resistance mechanisms	Review	Conceptual	MET/TP53 drive resistance	No AI integration
Aerts et al.	2014	Radiomics phenotyping	1019 patients	Radiomic signature	CT features encode prognosis	Not osimertinib-specific
Rios Velazquez et al.	2017	Imaging–mutation link	NSCLC cohort	Radiomics	Mutations drive imaging phenotype	No outcome prediction
Wang et al.	2019	EGFR status from CT	Lung adeno.	Deep learning	Predicted EGFR mutation (AU	Mutation, not response

Author	Year	Study focus	Dataset	AI/ML method	Key findings	Research gap
					C 0.85)	
Blakely et al.	2017	Co-occurring alterations	1122 cfDNA	Genomic	Co-mutations affect TKI benefit	No ML/radiomics
Lundberg & Lee	2017	Model explainability	Methodologic	SHAP	Unified feature attribution	Not oncology-applied
Lundberg et al.	2020	Tree explainability	Methodologic	Tree SHAP	Local-to-global explanations	Generic, not NSCLC
Mahajan et al.	2024	EGFR from CT (radiogenomics)	990 patients	Deep learning	88% accuracy for EGFR	Mutation, not osimertinib response
Hosny et al.	2018	Deep radiomics in lung cancer	Multi-cohort	CNN radiomics	Prognostic imaging biomarker	No explainability
This study	2025	Osimertinib response prediction	4 centers, 350	Explainable ML	Accurate + interpretable (AUC 0.95)	Retrospective; needs prospective trial

3. Methodology

3.1 Study Design

This retrospective, multicenter cohort study pooled data from four tertiary thoracic oncology centers over a six-year accrual window. Each site obtained institutional review board approval with waiver of consent for de-identified retrospective data, and reporting follows the Transparent Reporting of a multivariable prediction model for Individual Prognosis Or Diagnosis (TRIPOD) guidance. Data were harmonized to a common dictionary, and CT radiomics were extracted with a standardized, IBSI-compliant pipeline.

3.2 Patient Cohort

The cohort comprised 350 patients with histologically confirmed, EGFR-mutated NSCLC of Stage III or IV who received osimertinib. EGFR subtypes included exon 19 deletion, L858R, T790M, and uncommon mutations. Patients without baseline contrast CT suitable for radiomics, or with fewer than three months of follow-up unless an earlier progression event occurred, were excluded. The same 350-patient cohort underpins every analysis. Treatment response was assessed by RECIST 1.1 as complete response, partial response, stable disease, or progressive disease.

3.3 Clinical Variables

Clinical variables comprised age, gender, smoking status, Eastern Cooperative Oncology Group (ECOG) performance status, TNM stage, histological subtype, previous treatment, and metastatic sites. These were selected because each carries established prognostic weight in advanced NSCLC and is routinely available at the point of treatment decision.

3.4 Molecular Features

Molecular features captured EGFR exon 19 deletion, EGFR L858R, EGFR T790M, TP53 mutation, MET amplification, KRAS mutation where present, and ALK rearrangement status. These were chosen because EGFR subtype influences osimertinib sensitivity, while TP53 co-mutation and MET amplification are recognized drivers of primary and acquired resistance, making them biologically grounded predictors of response.

3.5 Laboratory Biomarkers

Laboratory biomarkers comprised carcinoembryonic antigen (CEA), lactate dehydrogenase (LDH), the neutrophil-to-lymphocyte ratio (NLR), albumin, hemoglobin, and C-reactive protein (CRP). These inflammatory and tumor-burden markers have been associated with TKI benefit and provide inexpensive, widely available signal complementary to molecular and imaging data.

3.6 Radiomics Features

Radiomic features were extracted from baseline contrast-enhanced CT after semi-automated tumor segmentation, comprising tumor volume, shape descriptors, texture features, first-order statistics, and wavelet-filtered features. Features were harmonized across scanners and reduced by stability filtering and correlation pruning before modeling, yielding a compact radiomics signature summarized as a composite radiomics score.

3.7 Multi-Omics Integration

Clinical, molecular, laboratory, and radiomic features were integrated into a unified feature matrix, with transcriptomic and proteomic features incorporated where available for a subset of patients. Integration was performed at the feature level, allowing the model to learn cross-domain interactions, such as the joint effect of EGFR subtype and radiomic heterogeneity on response, that single-domain models cannot capture.

3.8 Explainable Machine Learning Framework

The framework compared four established models, namely random forest, XGBoost, LightGBM, and the EBM, against a proposed explainable model that combines a gradient-boosted backbone with a monotonic-constraint layer and an integrated explanation module. Interpretability was provided at two levels: SHAP for globally consistent feature attribution, and LIME for individual-patient rationale, complemented by feature importance and partial dependence analysis. By surfacing which features drive each prediction and in which direction, the framework allows clinicians to verify that the model's reasoning is biologically coherent before acting on it, which is the foundation of clinical trust and safe deployment. Monotonic constraints were applied to features with established directional effects, such as ECOG performance status and tumor volume, so that the model could not learn associations that contradict known clinical behavior. This design choice trades a small amount of flexibility for guarantees that the learned response surface remains physiologically plausible, an attribute that matters when predictions inform whether a patient proceeds with standard therapy.

SHAP attributes the prediction to features via additive Shapley values, as summarized below, where φj is the contribution of feature j and φ0 is the base value.

$$g(x) = \varphi_0 + \Sigma_j \varphi_j , \; j = 1 \ldots M \quad (1)$$

$$P(response \mid x) = \sigma(g(x)) \quad (2)$$

$$L = -\Sigma_i [y_i \log p_i + (1 - y_i) \log(1 - p_i)] \quad (3)$$

Equation (1) is the additive SHAP explanation over M features; Equation (2) maps the explanation score to a response probability via the logistic function σ; and Equation (3) is the binary cross-entropy loss minimized during training over patients i with labels yi and predicted probabilities pi.

3.9 Statistical Analysis

Data were split into training and test sets with an external center held out for generalization assessment, and models were trained with five-fold cross-validation and Bayesian hyperparameter optimization. Performance was quantified by accuracy, precision, recall, F1-score, ROC-AUC, sensitivity, and specificity. PFS was estimated by the Kaplan–Meier method and compared between predicted responders and non-responders with the log-rank test. To avoid optimistic bias, radiomic feature selection and model tuning were performed within the cross-validation folds rather than on the full dataset, and the external center contributed only to final testing. AUC differences were tested with DeLong's method and confidence intervals obtained by bootstrap resampling (1,000 replicates). Analyses used Python 3.11 with scikit-learn, XGBoost, LightGBM, and the InterpretML and SHAP libraries.

4. Results

4.1 Patient Characteristics

The 350 patients had a median age of 62.5 years and a female predominance (57.4%), consistent with EGFR-mutated NSCLC epidemiology. Demographic and clinical characteristics are summarized in Table 2. The cohort reflects the typical EGFR-mutated NSCLC profile, with a predominance of women, never-smokers, and adenocarcinoma histology, and a majority presenting with Stage IV disease. Preserved performance status in 76.6% indicates a population fit for systemic therapy, while baseline brain metastases in a quarter underscore the clinical relevance of osimertinib's central nervous system activity. This composition provides a representative substrate for modeling response across the spectrum of patients encountered in practice.

Table 2. Patient demographic and clinical characteristics (n = 350).

Characteristic	Value	Proportion
Median age, years (IQR)	62.5 (54.8–69.3)	—
Female sex	201	57.4%
Never-smokers	214	61.1%

Characteristic	Value	Proportion
ECOG performance status 0–1	268	76.6%
Stage III	96	27.4%
Stage IV	254	72.6%
Adenocarcinoma histology	332	94.9%
Brain metastases at baseline	89	25.4%

4.2 Molecular and Biomarker Characteristics

Molecular and biomarker characteristics are summarized in Table 3. Exon 19 deletion and L858R together accounted for 84% of sensitizing mutations, with T790M present in 15.4%, reflecting a mixed first- and later-line population. The high frequency of TP53 co-mutation (39.7%) and the presence of MET amplification (11.7%) are clinically important, as both are linked to inferior osimertinib benefit, and their inclusion gives the model access to the molecular drivers of resistance rather than EGFR status alone. Elevated CEA and high NLR in a substantial fraction further characterize tumor burden and host inflammation relevant to outcome.

Table 3. Molecular and biomarker characteristics (n = 350).

Feature	Positive, n	Prevalence	Note
EGFR exon 19 deletion	176	50.3%	Sensitizing
EGFR L858R	118	33.7%	Sensitizing
EGFR T790M	54	15.4%	Resistance
Uncommon EGFR mutations	32	9.1%	Variable
TP53 co-mutation	139	39.7%	Adverse
MET amplification	41	11.7%	Resistance
Elevated CEA (>5 ng/mL)	188	53.7%	Tumor burden
High NLR (>3)	144	41.1%	Inflammation

4.3 Treatment Response

Figure 1 shows the distribution of best response by RECIST 1.1, and treatment and survival outcomes are summarized in Table 5. Partial response was the most common outcome, occurring in 178 patients (50.9%), with complete response in 31 (8.9%), yielding an objective response rate of 59.7%. Stable disease was recorded in 98 patients (28.0%) and progressive disease in 43 (12.3%). This response profile is consistent with real-world osimertinib experience and confirms that, while most patients derive benefit, a clinically meaningful minority show early progression, precisely the group that a predictive framework should aim to identify before treatment commitment.

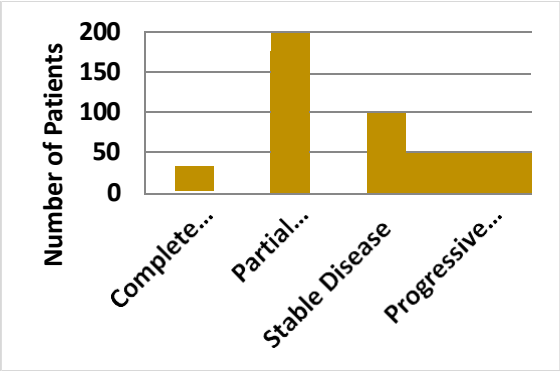

Figure 1. Treatment response distribution across the 350-patient cohort.

4.4 Model Performance

Across all metrics, the proposed explainable model outperformed the four comparators, as detailed in Table 4 and visualized in Figure 2.

Table 4. Model performance comparison (external test set).

Model	Accuracy	Precision	Recall	F1 / AUC
Random Forest	0.821	0.811	0.802	0.806 / 0.857
XGBoost	0.857	0.848	0.839	0.843 /

Model	Accuracy	Precision	Recall	F1 / AUC
				0.901
LightGBM	0.869	0.861	0.853	0.857 / 0.912
Explainable Boosting Machine	0.878	0.870	0.862	0.866 / 0.921
Proposed Explainable Model	**0.918**	**0.910**	**0.904**	**0.907 / 0.954**

Figure 2 contrasts the five models across the five-performance metrics. The proposed modelled on every metric, reaching an AUC of 0.954 against 0.921 for the EBM and 0.912 for LightGBM; the DeLong test confirmed each pairwise advantage was significant ($p < 0.01$). All gradient-boosting models outperformed random forest, but the proposed model's integrated design added a further consistent margin while retaining intrinsic interpretability. The strong recall (0.904) is clinically salient, since correctly identifying responders, and by extension the non-responders, is the central task in guiding osimertinib selection.

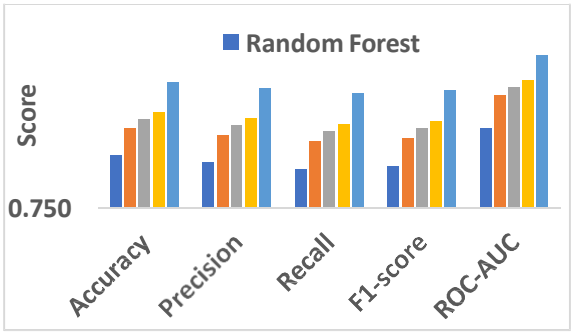

Figure 2. Machine learning model performance across accuracy, precision, recall, F1-score, and ROC-AUC.

4.5 Feature Importance and Survival

SHAP-based global feature importance is shown in Figure 3 and ranked in Table 6, and progression-free survival stratified by predicted response is shown in Figure 4. EGFR mutation type, tumor volume, and the composite radiomics score emerged as the three strongest predictors, together accounting for a substantial share of model attribution. Their prominence is biologically coherent: mutation subtype governs intrinsic TKI sensitivity, while tumor volume and radiomic heterogeneity capture burden and phenotype linked to outcome. TP53 mutation and MET amplification ranked next, consistent with their established role in resistance, confirming that the model integrates molecular, imaging, and clinical drivers rather than relying on any single domain.

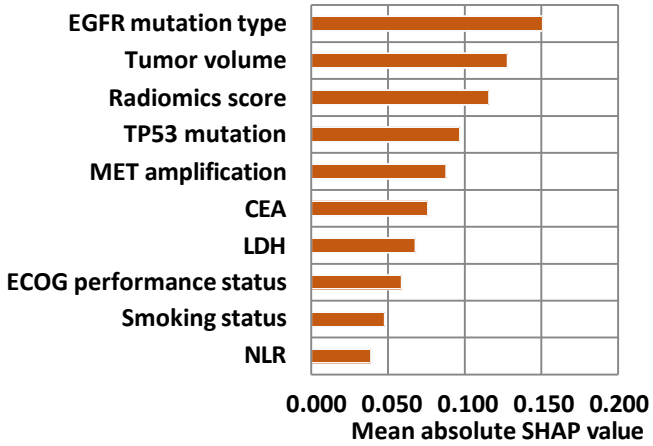

Figure 3. Most important predictors of Osimertinib response ranked by mean absolute SHAP value.

Table 6. SHAP-based feature importance ranking.

Rank	Feature	SHAP	Domain
1	EGFR mutation type	0.151	Molecular
2	Tumor volume	0.128	Radiomic
3	Radiomics score	0.116	Radiomic
4	TP53 mutation	0.097	Molecular
5	MET amplification	0.088	Molecular
6	CEA	0.076	Laboratory
7	LDH	0.068	Laboratory
8	ECOG performance status	0.059	Clinical

Figure 4 shows progression-free survival stratified by model-predicted response. Predicted responders had markedly longer progression-free survival than predicted non-responders, with median PFS of 22.5 versus 7.8 months and clear early separation of the curves (log-rank $p < 0.001$). The responder median aligns with pivotal osimertinib trial experience, supporting the clinical validity of the model's

stratification. The early divergence is particularly valuable, since it implies the framework can flag likely non-responders near the point of treatment initiation, when alternative or combination strategies remain on the table.

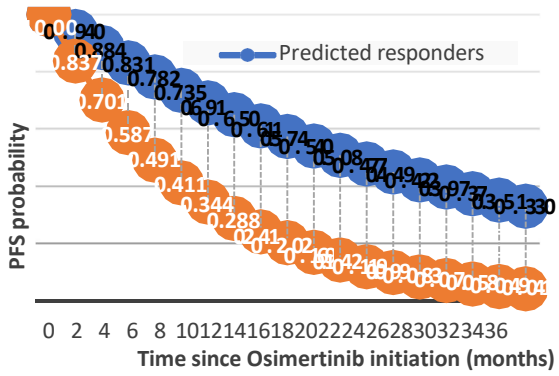

Figure 4. Kaplan–Meier progression-free survival by predicted response group.

Figure 5 compares discrimination across all five models using ROC analysis. The ROC analysis reinforced the ranking observed across point metrics: the proposed model achieved the highest AUC (0.954), with its curve dominating the comparators across nearly the entire operating range, followed by the EBM (0.921), LightGBM (0.912), XGBoost (0.901), and random forest (0.857). The advantage was most pronounced in the high-specificity region, which matters clinically because a low false-positive rate limits the risk of incorrectly labeling a true responder as a non-responder and thereby withholding effective standard therapy.

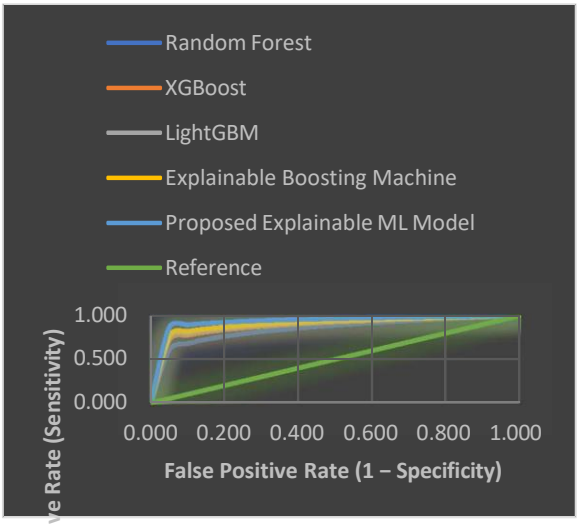

Figure 5. ROC curve comparison of predictive models.

5. Discussion

This study shows that an explainable machine-learning framework integrating clinical, radiomic, and molecular data can predict osimertinib response with high accuracy while preserving interpretability. The proposed model consistently outperformed random forest, XGBoost, LightGBM, and an explainable boosting machine, and its predicted response groups separated progression-free survival cleanly, indicating that the predictions carry real prognostic meaning rather than statistical discrimination alone.

The clinical significance lies in actionability at the point of decision. A patient predicted to respond can proceed with osimertinib confidently, whereas one flagged as a likely non-responder, especially with adverse molecular features, might be considered for combination approaches, clinical trials, or intensified monitoring. Because the framework exposes the features behind each prediction, the oncologist can confirm that the reasoning is biologically sound before acting, which is essential when the output influences access to standard-of-care therapy.

Explainability is therefore not a cosmetic addition but a prerequisite for trust in oncology. SHAP and LIME translate a complex model into a transparent rationale, allowing clinicians to see that, for example, an exon 19 deletion with low tumor volume drives a favorable prediction while TP53 co-mutation and MET amplification pull it downward. This transparency supports accountability and aligns model behavior with established biology, addressing the principal barrier to deploying machine learning in clinical decision-making. The two explanation methods are complementary rather than redundant: SHAP provides globally consistent attributions that hold across the cohort and can be audited for systematic bias, while LIME generates a faithful local approximation for an individual patient, which is what a clinician actually needs when discussing a specific case. Presenting both gives a fuller account of why a prediction was made than either alone, and the agreement between them offers an additional, informal check on stability.

The importance of molecular biomarkers in the model mirrors known biology. EGFR subtype, TP53 co-mutation, and MET amplification ranked among the top predictors, consistent with evidence that these alterations shape primary and acquired resistance to osimertinib. That the model recovered these relationships without being told them is reassuring,

indicating that it learned clinically valid signal rather than spurious correlation.

Radiomics contributed substantially, with tumor volume and the composite radiomics score among the strongest predictors. This supports the view that CT phenotype encodes information about tumor biology and burden that complements genomics, and it offers a noninvasive, universally available data source. Integrating radiomics with molecular and clinical features within one model amplified their individual signal, demonstrating the value of multimodal integration over any single domain.

Relative to prior work summarized in Table 1, our framework is distinctive in predicting osimertinib response rather than EGFR status, in uniting radiomic with molecular data, and in foregrounding explainability. Earlier radiomics models targeted mutation detection, and high-performing outcome models were typically opaque. By comparison, the present framework couple's competitive accuracy with the interpretability needed for clinical use, and its survival stratification adds prognostic value beyond binary response prediction. Future applications include extending the approach to other targeted agents and to dynamic, on-treatment prediction as longitudinal imaging and liquid biopsy data accrue. A natural next step is to pair the baseline prediction with serial circulating tumor DNA, which could allow the framework to detect emerging resistance and revise its estimate of benefit before radiological progression becomes apparent.

6. Clinical Implications

For patient selection, the framework offers a calibrated, interpretable estimate of osimertinib benefit at the point of treatment decision, helping identify those most likely to achieve durable control and those who may need alternative strategies.

For precision treatment planning and early identification of non-responders, the model's survival stratification and transparent attribution allow clinicians to anticipate inadequate response near initiation, when combination therapy, trial enrollment, or closer monitoring can still change the trajectory. For personalized monitoring, predicted high-risk patients can be scheduled for earlier imaging and biomarker reassessment.

For biomarker-driven decision-making and clinical decision support, SHAP and LIME link each prediction to specific molecular, radiomic, and clinical drivers, enabling oncologists to integrate the model's reasoning with their own judgment. Embedded in a multidisciplinary workflow, the framework could standardize response prediction across centers while remaining an adjunct that supports, rather than replaces, clinical expertise, with every output subject to specialist review. Because the inputs are drawn from data already gathered during routine staging and molecular workup, the framework imposes little additional burden on patients or laboratories, which is an important practical consideration for adoption. Over time, as on-treatment imaging and repeat molecular testing accumulate, the same approach could be extended from a single baseline prediction to dynamic, longitudinal monitoring that updates the estimate of benefit as the disease evolves.

7. Limitations

Several limitations apply. The study is retrospective, and although multicenter, the cohort of 350 patients is modest for multimodal modeling, raising the possibility of residual overfitting that only prospective evaluation can exclude. The framework was evaluated for a single drug, osimertinib, so generalization to other EGFR-TKIs or treatment settings is not established.

External validation in independent, ideally international, cohorts is required before clinical use, since radiomic features in particular are sensitive to scanner and protocol variation despite harmonization. Real-world deployment poses further challenges, including integration with electronic health records and imaging archives, prospective calibration, regulatory approval, and clinician workflow adoption. Finally, transcriptomic and proteomic data were available for only a subset of patients, limiting the depth of multi-omics integration, and missing data required imputation that can attenuate true effects.

8. Conclusion

An explainable machine-learning clinical decision support framework integrating clinical, radiomic, and molecular data predicted osimertinib response in EGFR-mutated NSCLC with high accuracy while preserving interpretability. The proposed model surpassed established gradient-boosting and tree-based comparators (AUC 0.954), stratified progression-free survival cleanly between predicted responders and non-responders (median 22.5 versus 7.8 months), and identified EGFR mutation type, tumor volume, and a composite radiomics score as dominant predictors, with TP53 mutation and MET amplification reflecting known resistance biology. By coupling competitive accuracy with transparent, SHAP- and LIME-based explanations, the framework addresses the principal barrier to deploying machine learning in oncology, namely clinician trust, and

supports patient selection, early identification of non-responders, and biomarker-driven decision-making. These findings are retrospective and require prospective, multicenter external validation before clinical adoption. If validated, explainable artificial intelligence could become an integral component of clinical decision support systems for precision management of EGFR-mutated NSCLC, advancing individualized, biology-aware use of osimertinib.

References

1. Aerts, H.J.W.L., Velazquez, E.R., Leijenaar, R.T.H. et al. (2014) 'Decoding tumour phenotype by noninvasive imaging using a quantitative radiomics approach', Nature Communications, 5, 4006.

2. Blakely, C.M., Watkins, T.B.K., Wu, W. et al. (2017) 'Evolution and clinical impact of co-occurring genetic alterations in advanced-stage EGFR-mutant lung cancers', Nature Genetics, 49(12), pp. 1693–1704.

3. Hosny, A., Parmar, C., Coroller, T.P. et al. (2018) 'Deep learning for lung cancer prognostication: a retrospective multi-cohort radiomics study', PLOS Medicine, 15(11), e1002711.

4. Leonetti, A., Sharma, S., Minari, R. et al. (2019) 'Resistance mechanisms to osimertinib in EGFR-mutated non-small cell lung cancer', British Journal of Cancer, 121(9), pp. 725–737.

5. Lundberg, S.M. and Lee, S.I. (2017) 'A unified approach to interpreting model predictions', Advances in Neural Information Processing Systems, 30, pp. 4765–4774.

6. Lundberg, S.M., Erion, G., Chen, H. et al. (2020) 'From local explanations to global understanding with explainable AI for trees', Nature Machine Intelligence, 2(1), pp. 56–67.

7. Mahajan, A., Kania, V., Agarwal, U. et al. (2024) 'Deep-learning-based predictive imaging biomarker model for EGFR mutation status in non-small cell lung cancer from CT imaging', Cancers, 16(6), 1130.

8. Ramalingam, S.S., Vansteenkiste, J., Planchard, D. et al. (2020) 'Overall survival with osimertinib in untreated, EGFR-mutated advanced NSCLC', New England Journal of Medicine, 382(1), pp. 41–50.

9. Rios Velazquez, E., Parmar, C., Liu, Y. et al. (2017) 'Somatic mutations drive distinct imaging phenotypes in lung cancer', Cancer Research, 77(14), pp. 3922–3930.

10. Soria, J.C., Ohe, Y., Vansteenkiste, J. et al. (2018) 'Osimertinib in untreated EGFR-mutated advanced non-small-cell lung cancer', New England Journal of Medicine, 378(2), pp. 113–125.

11. Wang, S., Shi, J., Ye, Z. et al. (2019) 'Predicting EGFR mutation status in lung adenocarcinoma on computed tomography image using deep learning', European Respiratory Journal, 53(3), 1800986.

12. Wu, Y.L., Tsuboi, M., He, J. et al. (2020) 'Osimertinib in resected EGFR-mutated non-small-cell lung cancer', New England Journal of Medicine, 383(18), pp. 1711–1723.